Chinese Journal of Natural Medicines

Notoginsenoside Ft1 inhibits colorectal cancer growth by increasing $CD8^+$ T cell proportion in tumor-bearing mice through the USP9X signaling pathway

Yutao FENG, Yuan LI, Fen MA, Enjiang WU, Zewei CHENG, Shiling ZHOU, Zhengtao WANG, Li YANG, Xun SUN, Jiwei ZHANG

Citation: Yutao FENG, Yuan LI, Fen MA, Enjiang WU, Zewei CHENG, Shiling ZHOU, Zhengtao WANG, Li YANG, Xun SUN, Jiwei ZHANG, Notoginsenoside Ft1 inhibits colorectal cancer growth by increasing $CD8^+$ T cell proportion in tumor-bearing mice through the USP9X signaling pathway, Chinese Journal of Natural Medicines, 2024, 22(4), 329-340. doi: 10.1016/S1875-5364(24)60623-0.

View online: https://doi.org/10.1016/S1875-5364(24)60623-0

Available online at www.sciencedirect.com
ScienceDirect
Chinese Journal of Natural Medicines 2024, **22**(4): 329-340
doi: 10.1016/S1875-5364(24)60623-0
Chinese Journal of Natural Medicines

•Original article•

Notoginsenoside Ft1 inhibits colorectal cancer growth by increasing CD8$^+$ T cell proportion in tumor-bearing mice through the USP9X signaling pathway

FENG Yutao[1Δ], LI Yuan[1Δ], MA Fen[1Δ], WU Enjiang[1], CHENG Zewei[1], ZHOU Shiling[1], WANG Zhengtao[1], YANG Li[1*], SUN Xun[2*], ZHANG Jiwei[1*]

[1] *Shanghai Key Laboratory of Compound Chinese Medicines, The MOE Key Laboratory for Standardization of Chinese Medicines, Institute of Chinese Materia Medica, Shanghai University of Traditional Chinese Medicine, Shanghai 201203, China;*
[2] *Gastrointestinal surgery, Longhua Hospital, Shanghai University of Traditional Chinese Medicine, Shanghai 200032, China*

Available online 20 Apr., 2024

[ABSTRACT] The management of colorectal cancer (CRC) poses a significant challenge, necessitating the development of innovative and effective therapeutics. Our research has shown that notoginsenoside Ft1 (Ng-Ft1), a small molecule, markedly inhibits subcutaneous tumor formation in CRC and enhances the proportion of CD8$^+$ T cells in tumor-bearing mice, thus restraining tumor growth. Investigation into the mechanism revealed that Ng-Ft1 selectively targets the deubiquitination enzyme USP9X, undermining its role in shielding *β*-catenin. This leads to a reduction in the expression of downstream effectors in the Wnt signaling pathway. These findings indicate that Ng-Ft1 could be a promising small-molecule treatment for CRC, working by blocking tumor progression *via* the Wnt signaling pathway and augmenting CD8$^+$ T cell prevalence within the tumor environment.

[KEY WORDS] Notoginsenoside Ft1; Colorectal cancer; CD8$^+$ T cell; Ubiquitin-specific peptidase 9 X-linked; *β*-Catenin; Wnt
[CLC Number] R965 **[Document code]** A **[Article ID]** 2095-6975(2024)04-0329-12

Introduction

Colorectal cancer (CRC) [1] ranks among the deadliest cancers globally. Despite the significant extension of patient survival achieved through first-line treatments such as radiotherapy, chemotherapy, and adjuvant chemotherapy, the clinical hurdles of metastasis, invasion, and drug resistance in CRC tumors persist as formidable challenges [2-6]. Consequently, the search for novel therapeutic agents constitutes a principal focus of CRC research. In the context of tumor immunotherapy, T cells play a pivotal role within the tumor immune microenvironment [7]. Studies have demonstrated that CD8$^+$ T cells, once activated *via* the T cell receptor signaling pathway, can penetrate tumor cells, secreting tumor necrosis factor-α and interferon-γ, thereby exerting cytotoxic effects on tumors [8, 9]. This has led to numerous immunotherapeutic strategies aiming to enhance CD8$^+$ T cells activity or increase their infiltration into tumors, as a means to curb tumor growth [10-12].

The Wnt family, comprising secreted signaling proteins, plays a critical role throughout human development, from embryonic stages to adulthood, and is crucial for CRC progression [13]. *β*-Catenin, at the heart of the Wnt signaling pathway, exhibits mutations in 48% of CRC cases. These abnormalities in *β*-catenin contribute to tumor heterogeneity and drug resistance [14, 15] and lead to the overactivation of downstream target genes such as *CD44*, *MMP-7*, *C-myc*, *C-jun* in the Wnt signaling pathway. This overactivation influences colorectal tumor proliferation, migration, and invasion [16].

Findings suggest that saponins from *Panax notoginseng* exhibit properties such as reducing swelling, alleviating pain, boosting immunity, and offering anti-inflammatory and anti-tumor benefits [17-21]. However, the effectiveness of *Panax notoginseng*'s extract, specifically notoginsenoside R1 (NGR1), in treating CRC and breast cancer remains underexplored [22, 23]. Given the immune-enhancing and low-toxicity benefits of saponins, identifying saponins capable of combating CRC is of paramount importance in addressing the current

[Received on] 10-Aug.-2023
[Research funding] This work was supported by Shanghai Pujiang Program (No. 20PJ1413000) and the National Natural Science Foundation of China (No. 82173106, 82130115, 81290108033, 82004004, and 82074011).
[*]**Corresponding author]** E-mails: yl7@shutcm.edu.cn (YANG Li); shsunxun@sina.cn (SUN Xun); joezhang@shutcm.edu.cn (ZHANG Jiwei)
[Δ]These authors contributed equally to this work.
These authors have no conflict of interest to declare.

challenges faced by CRC treatment.

In 2008, YANG Chongren *et al.* successfully isolated and identified the rare notoginsenoside Ft1 (Ng-Ft1) [24]. Preliminary *in vitro* studies have shown that Ng-Ft1 possesses anti-angiogenic properties, induces apoptosis, and inhibits cell proliferation in breast cancer and neuroblastoma cell lines, potentially through modulation of the Akt/mTOR pathway [25-27]. However, the therapeutic effects of Ng-Ft1 on CRC have been scarcely investigated. Our research demonstrates that Ng-Ft1 significantly impedes CRC growth in both in *vitro* and in *vivo* settings. RNA sequencing (RNA-seq) analysis revealed a substantial suppression of the Wnt signaling pathway by Ng-Ft1, while flow cytometry analysis indicated a notable increase in the proportion and effector function of $CD8^+$ T cells in a tumor-bearing model. Mechanistically, it was discovered that Ng-Ft1 directly interacts with ubiquitin-specific peptidase 9 X-linked (USP9X), thereby inhibiting the aberrant activation of the *β*-catenin downstream pathway and, consequently, the proliferation of CRC cells. These findings elucidate the pharmacological mechanism by which Ng-Ft1 counters CRC growth and offer new avenues for CRC treatment, potentially improving the prognosis for CRC patients.

Materials and Methods

Animal and cell lines

C57BL/6J and Balb/c mice, male, SPF grade, aged 6–8 weeks, and weighing 18 ± 2 g, were acquired from Spiff Corporation and subsequently housed under SPF conditions. The Experimental Animal Ethics Committee of the Shanghai University of Traditional Chinese Medicine has reviewed and approved all animal experiments, ensuring compliance with relevant animal ethics regulations. The MC38 and CT26 cell lines were sourced from Shanghai Zeye Biotechnology Co., Ltd., while the HT29 cell lines were kindly provided by Dr. YIN Chunzhao from the Chinese Academy of Sciences. The cells, at their logarithmic phase of growth, were cultured in DMEM (MA0212, Meilunbio) supplemented with 10% fetal bovine serum (FBS, C04001-500, Vivacell), 100 $U \cdot L^{-1}$ penicillin, and 100 $mg \cdot L^{-1}$ streptomycin (15140-122, Gibco), in an incubator with 5% CO_2 and saturated humidity at 37 °C. The study was conducted by the Declaration of Helsinki and approved by the Ethics Committee of the Affiliated Hospital of Jiangnan University (January 21, 2022 approval). The animal study protocol was approved by the Institutional Review Board of the Department of Laboratory Animal, Shanghai ZY (protocol code SHZY-202103311 and March 31, 2021 approval).

Drugs and reagents

Ng-Ft1 (catalogue No. BP1846) was sourced from Chengdu Purifa Technology Development Co., Ltd., Chengdu, China. 5-Fluorouracil (CAS No. 51-21-8) was obtained from Shanghai Yuanye Biotechnology Co., Ltd., Shanghai, China. WP-1130 (catalogue No. HY-13264) was procured from MedChemExpress, Shanghai, China. Dimethyl sulfoxide (DMSO) (catalogue No. 30072418) was purchased from Sinopsin Chemical Reagent Co., Ltd., Shanghai, China.

Cytotoxicity assay

Experiments were conducted using 96-well plates, into which suspensions of the MC38, HT29, and CT26 cell lines were inoculated (100 μL/well) with a seeding density of 5 000 cells per well. Following cell attachment, they were cultured and subsequently treated with the specified concentrations of drugs for a duration of 48 h. The cell viability was assessed using the CCK-8 assay kit (BS350A, Biosharp) according to the manufacturer's instructions. The absorbance at 450 nm was measured to determine the cell viability.

Cell proliferation assay

After enzymatic digestion, single-cell suspensions were prepared, counted, and adjusted to the desired concentration with a culture medium. These suspensions were then aliquoted into six-well plates, with each well containing 1000 cells. The clones were monitored for growth over a period of 9–14 days. Upon satisfactory clone development, the following steps were undertaken: The old medium was discarded from the six-well plate, and each well was washed twice with Phosphate-Buffered Saline (PBS). The residual PBS was carefully removed. 1 mL of methanol was added to each well for fixation and left to stand at room temperature for 10 min. The methanol was then aspirated, and the wells were allowed to air dry at room temperature. Cells were stained with 0.1 $mg \cdot mL^{-1}$ crystal violet and left at room temperature for 10 min. Excess crystal violet was removed, and the wells were washed under running water. After air drying at room temperature, the plates were scanned.

Cell migration experiment

Cells exhibiting robust growth were digested with trypsin. Subsequently, 2 mL of complete culture medium was used to resuspend the cells evenly. The cell suspension was then transferred to a 2 mL centrifuge tube and centrifuged at 2500 $r \cdot min^{-1}$ for 2 min. Using a 1 mL pipette tip, the supernatant was removed. The cell pellet was resuspended in 1 mL of serum-free DMEM medium for counting. Based on the count, the cell concentration was adjusted to 5×10^5/mL using a serum-free DMEM medium. A 24-well plate was prepared by adding 800 μL of complete medium into the central well, and a Transwell chamber was placed in this well. The cell suspension, having been adjusted to the appropriate concentration, was thoroughly mixed. Then, 200 μL of this suspension was added into the upper chamber of the Transwell. The required drug concentration was calculated and added accordingly. For each experimental condition, three replicates were set up to ensure the reliability of the results. Subsequently, the 24-well plates were returned to the incubator for a 24-hour incubation period. The methods used for staining and imaging were consistent with those employed in the cell growth experiments.

Tumor transplantation and treatment

Cells in the logarithmic growth phase were utilized to establish a subcutaneous tumor transplantation mouse model for CRC. Specifically, the MC38 cell suspension was pre-

pared at a concentration of 5×10^6/mL (for CT26 cells: 2.5×10^6/mL), and 0.2 mL of this suspension was injected subcutaneously into the right flank of each mouse under aseptic conditions. This procedure resulted in an inoculation of 1×10^6 MC38 cells or 5×10^5 CT26 cells per mouse. Mice were then routinely monitored and fed over a period of 7–11 d until the average tumor volume reached 80–100 mm^3. At this point, mice were randomly divided into three groups, each comprising five animals. For the treatment regimen, Ng-Ft1 was calculated at the dose of 10 and 30 $mg \cdot kg^{-1}$ body weight, while 5-fluorouracil (5-FU) was administered at dosages of 10 and 20 $mg \cdot kg^{-1}$ body weight. The control group received a vehicle solution consisting of normal saline with 1% DMSO, administered once daily. The experiment was concluded once the tumor volume in any mouse exceeded 2000 mm^3. Body weight and tumor volume were measured and recorded every three days. Upon termination of the experiment, tumors were excised, weighed, and processed for further analysis.

Flow cytometry

The tumor tissue was sectioned, lysed, and subsequently processed for immunostaining. Flow cytometry analysis was carried out following the guidelines specified by the Invitrogen eBioscience essential phenotyping kits. The specific antibodies utilized for this purpose included CD8 (AF700, Biolegend, catalogue No. 100730), CD4 (BV510, Biolegend, catalogue No. 100559), CD45 (FITC, Biolegend, catalogue No. 157608), TNF-α (PE, BD, catalogue No. 506306), IFN-γ (BV421, BD, catalogue No. 505829).

Mouse $CD45^+$ cell sorting

The tumor tissues were excised and immediately placed in a Roswell Park Memorial Institute (RPMI) culture medium. These tissues were subsequently subjected to mechanical disruption followed by enzymatic digestion using a solution containing 0.3 $mg \cdot mL^{-1}$ DNase I (Sigma-Aldrich) and 0.25 $mg \cdot mL^{-1}$ Liberase TL (Roche) in serum-free RPMI medium. The digestion process occurred in a CO_2 incubator at 37 °C for 30 min. Post-digestion, the tissues were passed through a 40 μm cell strainer (BD Biosciences) to eliminate tissue debris and obtain a single-cell suspension. These isolated cells were then washed and resuspended in Hank's balanced salt solution (HBSS) supplemented with 1% FBS in preparation for staining and multi-color flow cytometry analysis. For the specific examination of immune cells, $CD45^+$ cells from mice bearing MC38 tumors were isolated using a BD Aria III flow cytometer. The isolated $CD45^+$ cells were then processed for 5'-single-cell RNA sequencing (scRNA-seq) using the 10× Genomics platform. The antibody panel utilized for this analysis was consistent with those employed in the previously mentioned flow cytometry protocol.

Whole tumor tissues 3' library single-cell RNA sequencing

For the single-cell RNA sequencing process, the prepared cell suspension was loaded onto Chromium microfluidic chips for barcoding, utilizing the Chromium Controller (10× Genomics) with 3' chemistry. Subsequently, RNA extracted from the barcoded cells underwent reverse transcription. This step was followed according to the protocols provided with the Chromium Single Cell 3' Version 3 Reagent Kit, as specified by the manufacturer. The final step involved sequencing the library, which was performed on an Illumina sequencing platform.

Analysis of single-cell RNA-seq data

The scRNA-seq data obtained from the 10× Genomics platform were processed using CellRanger (version 6.0.2) with alignment and quantification performed against the mm10 mouse reference genome. This process resulted in the generation of a raw gene expression matrix for each scRNA-seq sample by CellRanger. Subsequently, the Seurat R package was employed for the identification of major cell types within the samples. Data normalization was achieved through the NormalizeData function within Seurat, adjusting for variations in gene expression levels across cells. To identify patterns and variations within the dataset, 3000 highly variable genes were selected for principal component analysis (PCA). The analysis focused on the top 30 principal components to elucidate the main axes of variation and to denoise the dataset. Cell clustering was conducted using an unsupervised graph-based clustering algorithm, leveraging the expression profiles of cells to group them based on similarities. For visual representation of the data, Uniform Manifold Approximation and Projection (UMAP) dimensionality reduction was applied utilizing the RunUMAP function within Seurat, facilitating the visualization of complex data in a two-dimensional space. The cluster-specific marker genes were identified by running the FindAllMakers function with default parameters.

Analysis of RNA-seq data

Differential gene expression analysis of the RNA-seq data was conducted using DESeq2. Following the identification of these genes, functional gene enrichment analysis was carried out using Metascape (https://metascape.org). Additionally, RNA-seq data from colorectal cancer patients obtained from the TCGA (The Cancer Genome Atlas) database was utilized to examine signal regulation concerning the differential expression of USP9X.

Immunofluorescence cell staining

The cells were fixed with 4% paraformaldehyde and permeabilized with 0.1% Triton X-100. Subsequently, they incubated overnight with USP9X Rabbit monoclonal antibody (mAb) (A9782, Abclonal) and *β*-Catenin Rabbit mAb (A19657, Abclonal) at a 1∶200 dilution at 4 °C. For detection, phycoerythrin (PE)-conjugated secondary antibody at a 1∶200 dilution was employed.

RT-qPCR

Total RNA was extracted from tumor tissues and cells, after which reverse transcription was conducted, followed by relative quantitative PCR according to the Vazyme protocol. Primers for the PCR were sourced from PrimerBank, with the specific reagents and sequences detailed in Table S1. The expression levels of mRNA were normalized against the *β-actin* gene.

Western blotting and immunoprecipitation

Proteins were extracted from cells and tissues using ra-

dioimmunoprecipitation assay (RIPA) lysate (P0013B, Beyotime), and their concentrations were determined using a Bicinchoninic Acid (BCA) Protein Assay Kit (BL521A, Biosharp). The proteins were then separated by 6% Sodium dodecyl-sulfate polyacrylamide gel electrophoresis (SDS-PAGE) gel and electroblotted onto NC (nitrocellulose) membranes. Each membrane was blocked for 1.5 h with 5% skim milk to prevent non-specific binding. The membranes were subsequently incubated with specific primary antibodies, followed by incubation with secondary antibodies. The immunereactive bands were detected using an ECL (enhanced chemiluminescence) luminescence solution (Service-bio) for visualization.

For immunoprecipitation studies, cell or tissue extracts were incubated with anti-USP9X antibodies at 4 °C overnight, followed by precipitation with protein Sepharose beads for another overnight period. The levels of USP9X/*β*-catenin complexes were then assessed by Western blotting analysis. The specific antibodies utilized for these procedures are detailed in Table S1.

Biotin-labeled pulldown assay

To prepare for the experiment, the fixed streptavidin gel was first equilibrated. Subsequently, 300 μL of a 5 mmol·L^{-1} solution of biotin and biotin-labeled notoginsenoside Ft1 were added to the tube under gentle agitation. The mixture was incubated at 4 °C for 60 min with mild shaking on a rotating platform. Following incubation, 250 μL of a biotin-blocking solution was introduced to the tube, thoroughly mixed, and then incubated at room temperature for 5 min. The gel was washed twice with Tris-buffered saline (TBS) buffer. Next, 300 μL of cell lysate containing total protein (1.5 mg) was added to the tube and incubated overnight at 4 °C with gentle rotation. At the end of the incubation period, the mixture was centrifuged at 1250 *g* for 60 s, and the supernatant was carefully transferred along with the beads into a new 1.5 mL centrifuge tube. Following centrifugation, 210 μL of the supernatant was discarded, leaving the bead pellet. The beads were then resuspended in 50 μL of 2× loading buffer. This mixture was thoroughly vortexed, heated in a boiling water bath for 5 min, and subsequently cooled on ice. Electrophoresis was conducted at 80 V using a 12% separation gel. Once the sample migrated to the interface between the stacking and separating gels, electrophoresis was halted. The gel segment corresponding to the sample was excised for mass spectrometry analysis, facilitating the identification of bound proteins.

Microscale thermophoresis

To commence the experiment, the recombinant USP9X was diluted to a concentration of 200 nmol·L^{-1} using PBS with 0.05% Tween-80 as a protein buffer. This solution, totaling 98 μL, was then mixed with 2 μL of a specific dye and incubated for 30 min at 25 °C. Following the incubation, the mixture was centrifuged at 12 000 r·min^{-1} for 10 min to separate the components, with the supernatant being reserved for subsequent steps. For the preparation of serial dilutions, 20 μL of a 400 μmol·L^{-1} Ng-Ft1 solution was added to the first of 16 PCR tubes. The next 15 tubes were filled with 10 μL PBS containing 0.05% Tween 80. A meticulous transfer of 10 μL from the first tube to the second was carried out, ensuring thorough mixing through pipetting. This process was repeated sequentially through to the last tube to achieve a dilution series of Ng-Ft1. Subsequently, 10 μL of the previously prepared recombinant USP9X protein supernatant was added to each of the 16 PCR tubes, followed by thorough mixing through pipetting. After allowing these mixtures to incubate at room temperature for 30 min, the samples were loaded into standard capillaries for the Monolith NT.115 instrument. The instrument was then set up by adjusting the red LED power to 100% and the MST power to 20%. A capillary scan was performed before starting the measurement. Once the measurements were completed, data analysis was conducted using the MO. Analysis software provided by Nanotemper. This included fitting the thermophoresis data to the Kd model to calculate the binding affinity (K_d) of the interaction. The specific recombinant proteins and reagents utilized throughout this experimental procedure were detailed in Table S1, ensuring clear documentation and reproducibility of the study.

Statistical analysis

Cell assays were conducted with at least three replicates, while in *vivo* data comprised at least five separate experiments. All experimental results were presented as the mean ± SEM (standard error of the mean). Statistical analysis was performed using GraphPad Prism 9 (GraphPad, San Diego, California). To evaluate the significance between various datasets, unpaired *t*-tests or one-way analyses of variance (ANOVA) were employed. A *P*-value of 0.05 or higher was considered not significant, whereas a *P*-value of 0.05 or lower was deemed significant.

Results

Ng-Ft1 inhibits the growth of CRC cells in vitro

We assessed the cytotoxicity effects of Ng-Ft1 on CRC cell lines CT26, MC38, and HT29 (Fig. 1A–1C). In comparison to 5-FU, which showed IC_{50} values of 0.171, 0.169, and 0.184 μmol·L^{-1}, respectively, Ng-Ft1 exhibited a less potent direct cytotoxic effect on CRC cells, with IC_{50} values of 30.75, 32.87, and 27.59 μmol·L^{-1}, respectively. Migration assays demonstrated that Ng-Ft1 significantly reduced the migratory capabilities of the MC38 and CT26 cell lines (Fig. 1D and 1F). Furthermore, proliferation assays indicated that Ng-Ft1 markedly suppressed the growth of MC38 cells (Fig. 1E and 1G). Considering the greater impact of Ng-Ft1 on cellular behaviors beyond mere cytotoxicity, these findings suggest that Ng-Ft1 may influence the biological functions of CRC cells through mechanisms other than direct cytotoxic effects.

Ng-Ft1 significantly inhibits the progression of CRC in vivo

In our study, we treated MC38 subcutaneous tumors in C57BL/6J mice and CT26 subcutaneous tumors in Balb/c

mice with Ng-Ft1. Over a period of 24 d, administration of 30 mg·kg^{-1} Ng-Ft1 significantly inhibited the growth of MC38 tumors, reducing both tumor volume and weight. This experiment, which included both high (30 mg·kg^{-1}) and low (10 mg·kg^{-1}) doses of Ng-Ft1, demonstrated that the anti-tumor efficacy of Ng-Ft1 at the higher concentration surpassed that of the 5-FU positive control group (Fig. 2A−2E). A similar level of efficacy was observed in the CT26 subcutaneous model (Fig. 2F−2I). Specifically, the 30 mg·kg^{-1} Ng-Ft1 group exhibited a significant tumor-suppressive effect, in contrast to the minimal impact observed with the 10 mg·kg^{-1} dosage. When compared to treatment groups receiving the first-line chemotherapy drug 5-FU, the 30 mg·kg^{-1} Ng-Ft1 group displayed comparable efficacy but induced minimal weight loss (Fig. 2H), suggesting that a 30 mg·kg^{-1} dosage of Ng-Ft1 may result in fewer adverse reactions than 5-FU. Additionally, hematoxylin-eosin staining of the vital organs from treated mice revealed that Ng-Ft1 administration did not alter the morphology of critical organs such as the liver and kidneys (Fig. S1).

Ng-Ft1 plays an anti-CRC function by enhancing T cell immunity

To elucidate the pharmacological mechanism of Ng-Ft1, we performed RNA sequencing on tumor-bearing tissues from C57BL/6J mice. This analysis identified a total of 547 genes with differential expression. Among these, the gene encoding the chemokine CXCR6 was significantly upregulated (Fig. 3A). Recent studies have indicated that CXCR6 is selectively expressed on CD8$^+$ T cells within tumor tissues [11], and CD8$^+$ T cells exhibiting high CXCR6 have demonstrated enhanced anti-tumor effects. Further investigation of the sequencing results through Gene Ontology (GO) and Kyoto Encyclopedia of Genes and Genomes (KEGG) enrichment analyses revealed that most signaling pathways associated with T cell differentiation, selection, and positive activation—which promote immune response—were uniformly upregulated in the Ng-Ft1 treatment group (Fig. 3B). IMoreover, the Wnt signaling pathway was identified as the most significantly downregulated pathway following Ng-Ft1 administration (Fig. 3C). These findings suggest that Ng-Ft1 may exert its therapeutic effects by augmenting the immune response mediated by T cells.

To gain a deeper understanding of the changes in immune cell subsets following Ng-Ft1 administration, we performed single-cell RNA sequencing on tumor-bearing tissues from C57BL/6J mice. By identifying cluster markers, we were able to analyze the composition of immune cells, including CD4$^+$ T cells, CD8$^+$ T cells, Dendritic cells, macrophages, monocytes, natural killer T cells, and neutrophils (Fig. 4A). The results showed an increase in CD8$^+$ T cell infiltration within the tumor tissues after Ng-Ft1 treatment, highlighting Ng-Ft1's capacity to enhance the activity of CD8$^+$T cells (Fig. 4B and 4C). This observation underscores the potential of Ng-Ft1 to boost the immune response against tumors by specifically promoting CD8$^+$ T cell infiltration.

To further investigate the impact of Ng-Ft1 on immune regulation, we utilized flow cytometry to examine immune cell clusters in tumor-bearing tissues of C57BL/6J mice. Our analysis revealed that, compared to the control group, Ng-Ft1 administration significantly increased the proportion of CD8$^+$ T cells (Fig. 4D and 4E). Within the CD8$^+$ T cell population, Ng-Ft1 treatment markedly enhanced the ratio of cells expressing TNF-α and IFN-γ (Figs. 4F and 4G). These findings indicate that Ng-Ft1 primarily augments tumor immunity by promoting CD8$^+$ T cell infiltration within CRC tissue and by amplifying the tumor-killing capabilities of these cells.

USP9X is a direct target of Ng-Ft1 in CRC cells

In the tumor microenvironment (TME), significant interaction and communication occur between the tumor cells and the immune system [28-30]. To delve deeper into the effects of Ng-Ft1 on CRC, biotin-labeled Ng-Ft1 was utilized to isolate interacting proteins from the lysates of the MC38 cell line. This approach enabled the identification of over 483 potential Ng-Ft1 binding proteins through mass spectrometry (Fig. 5A). Among these identified proteins, HSD17B4, TUBB5, and USP9X were highlighted as the top three candidates (Fig. 5B). To determine the most likely drug target among these three candidates, we consulted the TCGA database to assess the impact of differential expression of these proteins on the clinical prognosis of patients. Notably, a strong correlation was observed between the elevated expression of USP9X and poor patient prognosis (Fig. 5C). Additionally, the binding interaction between USP9X and Ng-Ft1 was confirmed *in vitro* through Microscale Thermophoresis (MST), demonstrating that Ng-Ft1 specifically binds to USP9X (Fig. 5D). The affinity constant measured from this interaction suggests that Ng-Ft1 exhibits a strong binding affinity towards USP9X, comparable to the level of antigen-antibody interactions.

USP9X is a member of the deubiquitinating enzyme family, which participates in the deubiquitination of various proteins and influences different roles across multiple human tumor types by stabilizing substrates such as *β*-catenin, FBXW7, TGF-β receptor 2, and SMAD4 [31-34]. The experiments conducted have demonstrated that USP9X is a direct binding target of Ng-Ft1 in CRC cells. Relative to the control group, transcription levels of USP9X in Ng-Ft1-treated MC38 tumor tissues were significantly reduced (Fig. 5E). This finding was further corroborated by evaluating the transcript levels of USP9X in clinical surgical samples from CRC patients, where USP9X transcription was notably higher in CRC tissues compared to adjacent non-tumorous tissues (Fig. 5F). The impact of Ng-Ft1 on USP9X expression was also assessed at the protein level in mouse tumor tissues using western blotting analysis. Results indicated that USP9X protein levels were decreased following Ng-Ft1 treatment (Fig. 5G). Additionally, immunohistochemical analysis of MC38 tumor-bearing tissue from Balb/c mice confirmed that Ng-Ft1 treatment significantly reduced the protein levels of USP9X (Fig. 5H).

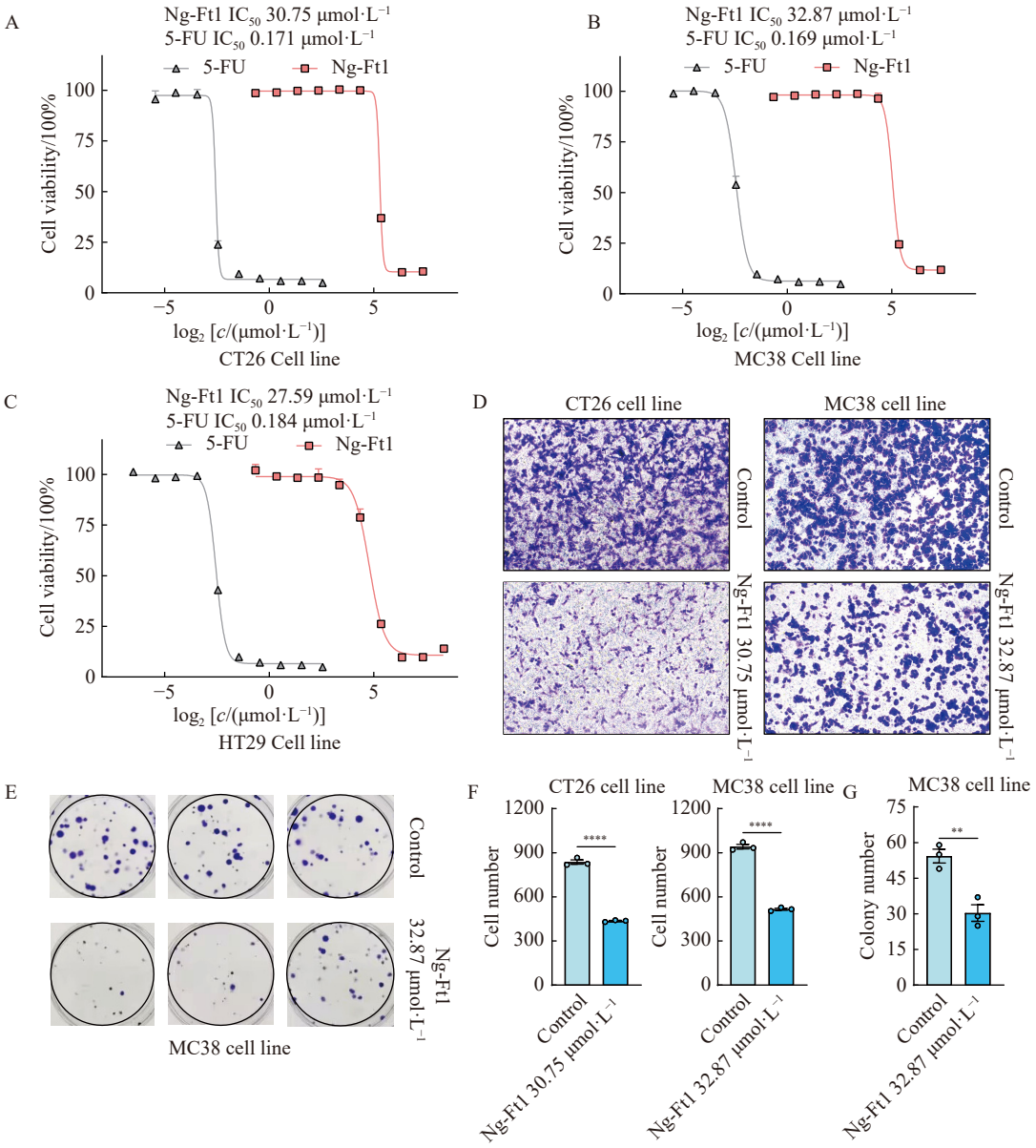

Fig. 1 Ng-Ft1 inhibits the growth of CRC cells *in vitro*. (A–C) Cell viability of MC38, CT26, HT29 cell line after Ng-Ft1 treatment at a concentration range from 0.625 to 320 μmol·L^{-1} after 72 h. (D, F) Cell migration assay of MC38, CT26 cell line with Ng-Ft1 at a concentration of IC_{50}. (E, G) Cell proliferation assay of MC38 cell line with Ng-Ft1 at a concentration of IC_{50}. Cells are resuscitated into a 6-well plate with Ng-Ft1 at a concentration of IC_{50}. Each well is transplanted with 1000 cells. Clone formation is observed after 10 d of incubation. Data are presented as means ± SEM (n = 3). $^{**}P < 0.01$; $^{****}P < 0.0001$.

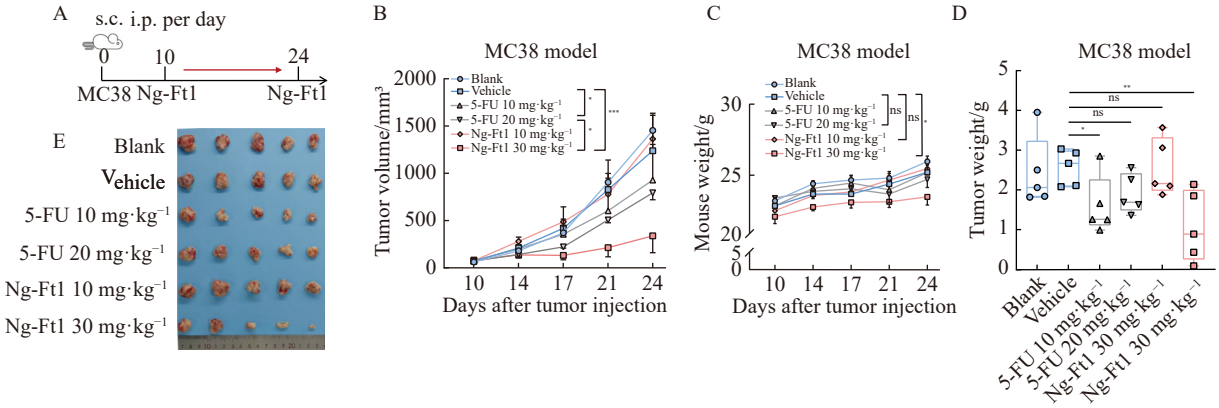

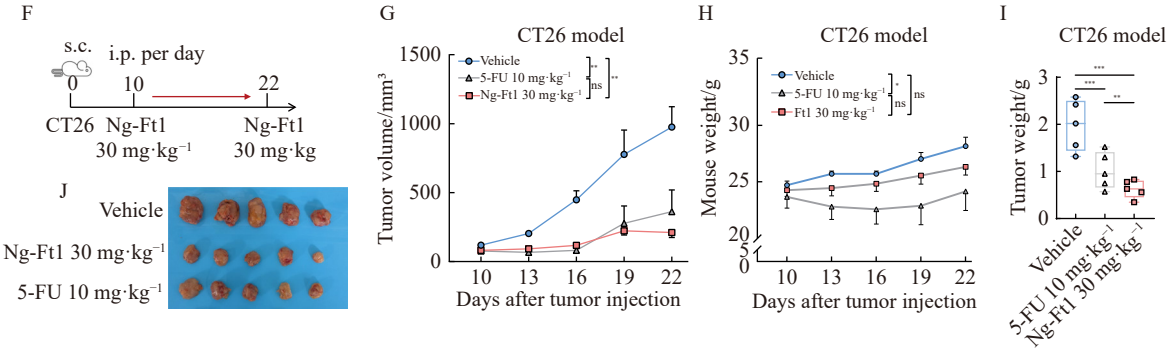

Fig. 2 Ng-Ft1 significantly inhibits the progression of CRC *in vivo*. Ng-Ft1 suppresses CRC cancer growth of tumor-bearing mice. (A) A total of 1 × 10^6 MC38 cells are separately injected into the right back of C57BL/6J mice. Mice are randomly divided into blank groups, vehicle groups, 5-FU 10 mg·kg^{-1} group, 5-FU 20 mg·kg^{-1} group, Ng-Ft1 10 mg·kg^{-1} group, and Ng-Ft1 30 mg·kg^{-1} group, (n = 5/group). (B) MC38 tumor growth is measured. (C) Mouse weights are measured. (D) Tumor weights of 6 groups are measured. (E) When the experiment is terminated, the MC38 model is dissected, and the tumor-bearing tissue is taken out and photographed. (F) A total of 5 × 10^5 CT26 cells are separately injected into the right back of the Balb/c mouse. Mice are randomly divided into a control group, Ng-Ft1 30 mg·kg^{-1} group, and 5-FU 10 mg·kg^{-1} group (n = 5/group). (G) CT26 tumor growth is measured. (H) Mouse weights are measured. (I) CT26 tumor weight of 3 groups is measured. (J)When the experiment is terminated, the CT26 mice model is dissected, and the tumor-bearing tissue is taken out and photographed. Data are presented as means ± SEM. ns, $P > 0.05$; $^{*}P < 0.05$; $^{**}P < 0.01$.

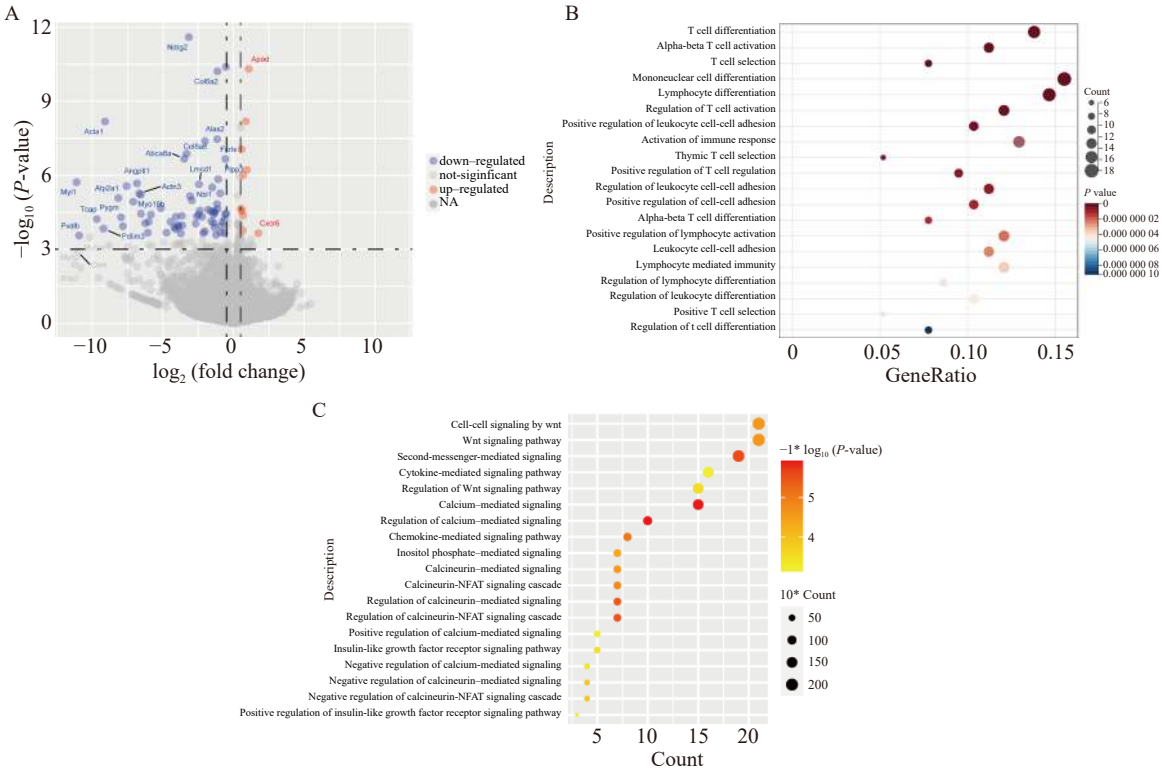

Fig. 3 Ng-Ft1 affects tumor immune-related signaling pathways. Transcriptome sequencing shows the transcriptome changes of tumor-infiltrating immune cells after treatment. (A) Volcano map of transcriptome sequencing. (B) GO plot from RNA-seq up-regulated differential gene expression profile. (C) GO plot from RNA-seq down-regulated differential gene expression profile.

Ng-Ft1 inhibits Wnt pathway activity by disrupting interactions between USP9X and β-catenin

We further explored the signaling pathways associated with USP9X upregulation in CRC using the TCGA CRC database [35], finding a strong correlation with the Wnt signaling pathway (Fig. 6A). Previous studies have established that USP9X can preserve Wnt signal transduction by stabilizing β-catenin. It achieves this by binding directly to β-catenin and preventing its polyubiquitination and subsequent degradation [31]. Our investigations revealed that treatment with Ng-Ft1 led to a decrease in β-catenin protein expression in CT26 cells, according to western blotting analyses (Fig. 6B). β-

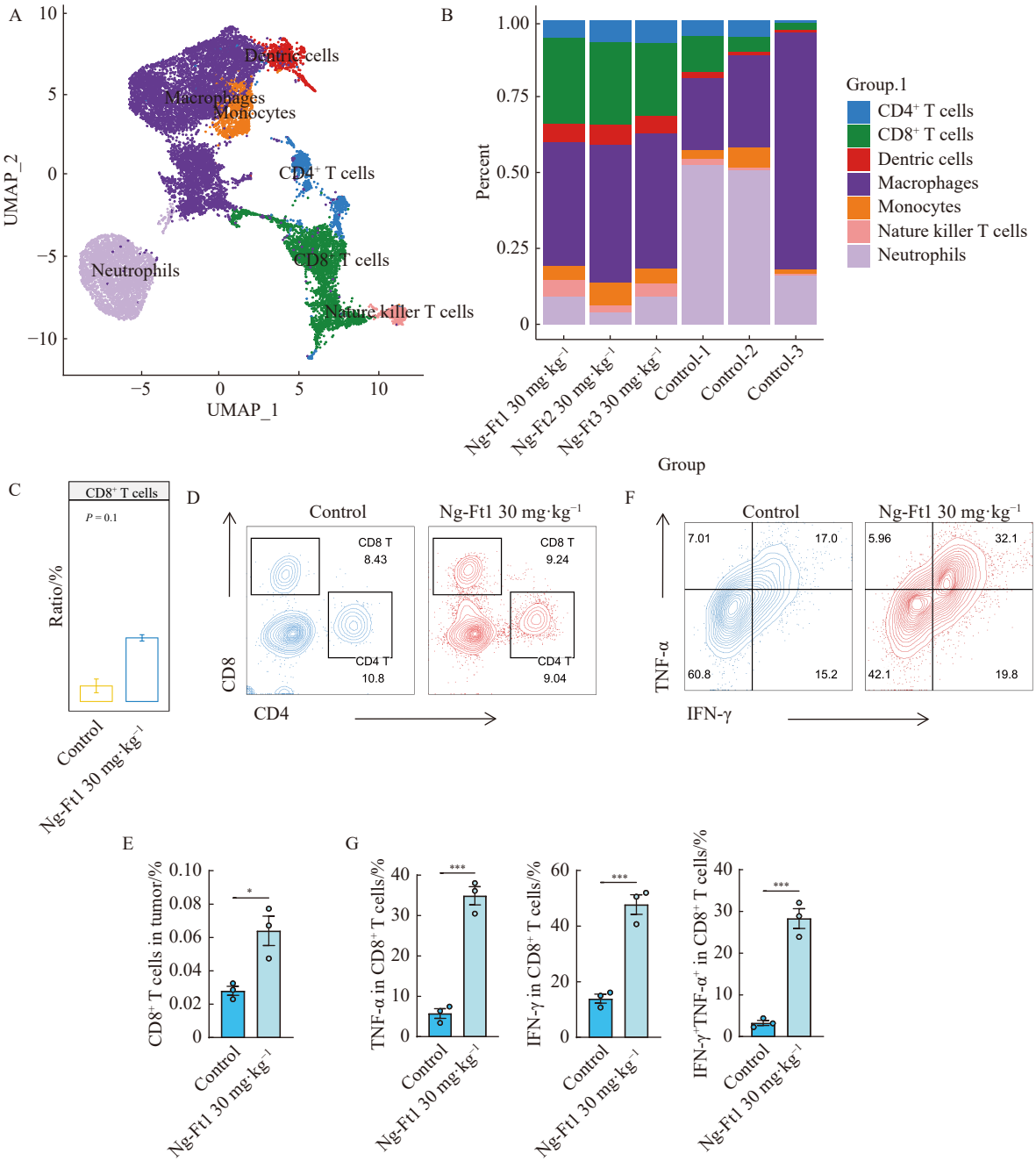

Fig. 4 Ng-Ft1 plays an anti-CRC function by enhancing T cell immunity. Single-cell RNA sequencing and flow cytometry are used to detect immune cell clusters in C57 mouse tumor-bearing tissues. (A) scRNA-seq UMAP projection of single cells from 6 tumor-bearing tissues. (B, C) Percentage (%) of the different immune clusters (B) and CD8$^+$ T cells (C) based on scRNA-seq data. (D, F) The proportion of tumor-infiltrating CD8$^+$ T cells in the Ng-Ft1 group and control group. (E, G) The proportion of TNF-α and IFN-γ expression in tumor-infiltrated CD8$^+$ T cells in the Ng-Ft1 group and control group. Data are presented as means ± SEM (n = 3). $^*P < 0.05$; $^{***}P < 0.001$.

catenin, when not degraded, translocates into the nucleus and binds to the co-transcription factor TCF-1, initiating the transcription of genes such as *CD44* and *MMP7*. This process contributes to the invasion and migration of tumor cells and initiates the transcription of C-myc, which promotes angiogenesis and regulates the tumor cell cycle and growth [16]. Through a co-immunoprecipitation (Co-IP) assay, we examined the interaction between USP9X and *β*-catenin, finding that Ng-Ft1 treatment disrupts their binding (Fig. 6C). Immunofluorescence studies on tumor-bearing mouse tissues also demonstrated the co-localization of USP9X with *β*-catenin, an interaction inhibited by Ng-Ft1 treatment, suggesting that Ng-Ft1 disrupts USP9X's function in stabilizing *β*-catenin (Fig. 6D). To verify whether Ng-Ft1's interference

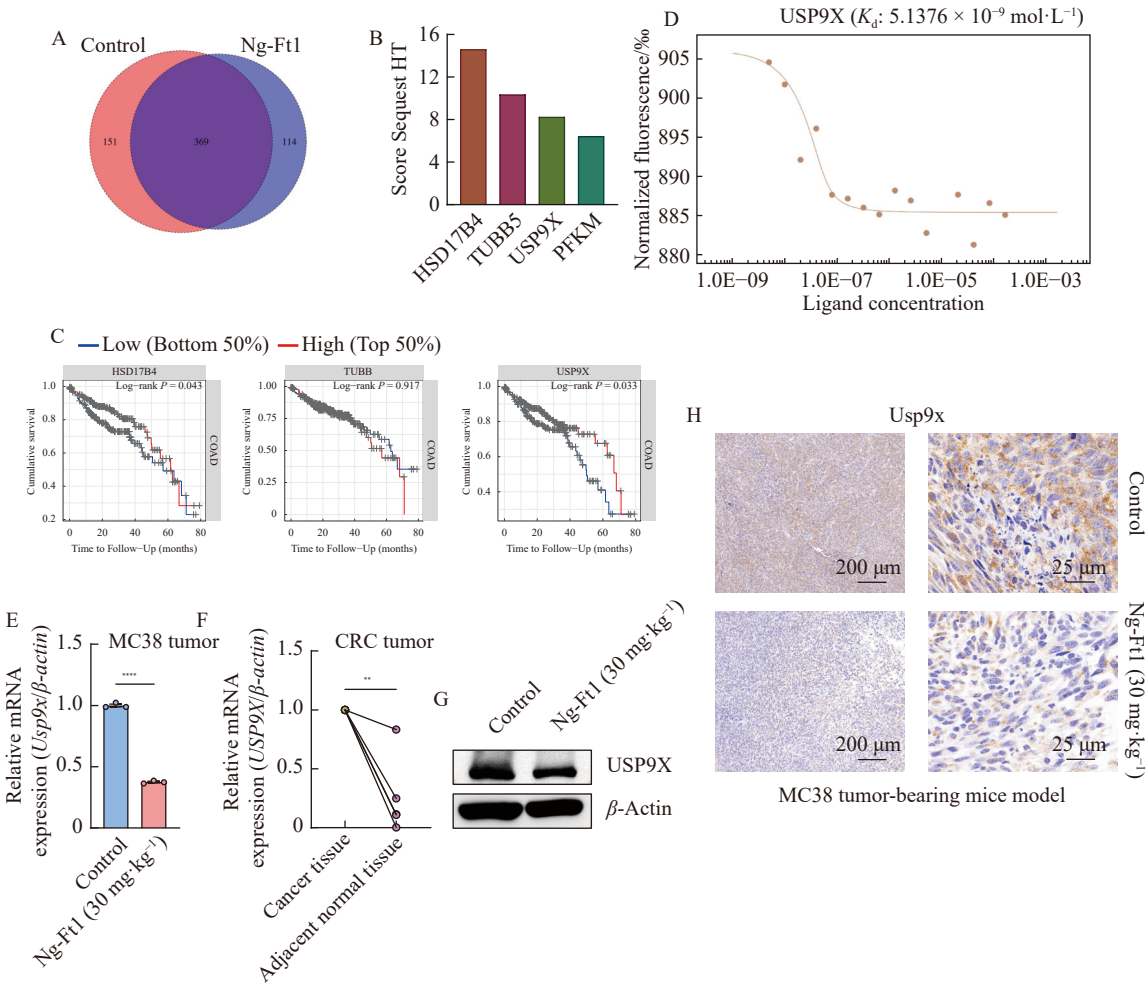

Fig. 5 USP9X is a direct target of Ng-Ft1 in CRC cells. (A, B) Biotin-marked Ng-Ft1 pulldown assay shows different protein peptides-related binding. (C) The correlation of candidate molecules with COAD patient survival is analyzed using TIMER 2.0. (D) MST detects specific binding of deubiquitylation enzyme USP9X to Ng-Ft1. (E) Total *Usp9x* transcription levels are evaluated in mouse MC38 tumor tissues. (F) Total *Usp9x* transcription levels are evaluated in CRC tissues. (G, H) Total USP9X protein expression levels are evaluated in mouse tumor tissues by Western blotting and immunohistochemistry. Data are presented as means ± SEM (n = 3). $^{**}P < 0.01$; $^{****}P < 0.0001$.

with USP9X impacts *β*-catenin signaling, RT-qPCR was utilized to examine the effect of Ng-Ft1 on target genes of the Wnt signaling pathway. We observed that Ng-Ft1 treatment significantly reduced the transcription levels of *Mmp7* and *Tcf7* (Fig. 6E). Additionally, western blotting analysis showed that the protein levels of MMP7 and TCF-1 were also reduced following Ng-Ft1 treatment (Fig. 6F). These findings collectively suggest that Ng-Ft1 binds specifically to USP9X in CRC cells, removes USP9X's protection of *β*-catenin, and subsequently inhibits downstream regulators of the Wnt signaling pathway (Fig. 7).

Discussion

Expanding treatment options for CRC is essential to enhance patient outcomes. A critical strategy toward this goal involves the exploration of effective natural compounds. Ng-Ft1, derived from *Panax notoginseng*, has traditionally been used in herbal concoctions to promote blood circulation and alleviate blood stasis in the treatment of surgical conditions. To date, pharmacological studies on the effects of Ng-Ft1 on CRC have been lacking. Our research marks the first demonstration of Ng-Ft1's therapeutic benefits in a CRC mouse model. As a small molecule originating from the natural product (NP) *Panax notoginseng*, Ng-Ft1 has shown superior efficacy compared to 5-FU in treating mouse CRC, with the added advantage of reduced adverse effects. This highlights Ng-Ft1's potential for further development as a chemotherapeutic agent. RNA-seq analysis of the MC38 subcutaneous tumor model treated with Ng-Ft1 revealed a significant disruption of the Wnt/*β*-catenin signaling pathway, suggesting that the inhibition of this pathway may underlie Ng-Ft1's mechanism of action against CRC. The Wnt/*β*-catenin pathway has been recognized as a viable target for the pharmacotherapy of various tumors [36]. However, the pursuit of targeting this pathway in clinical trials has underscored the necessity of addressing the associated risks of side effects and off-

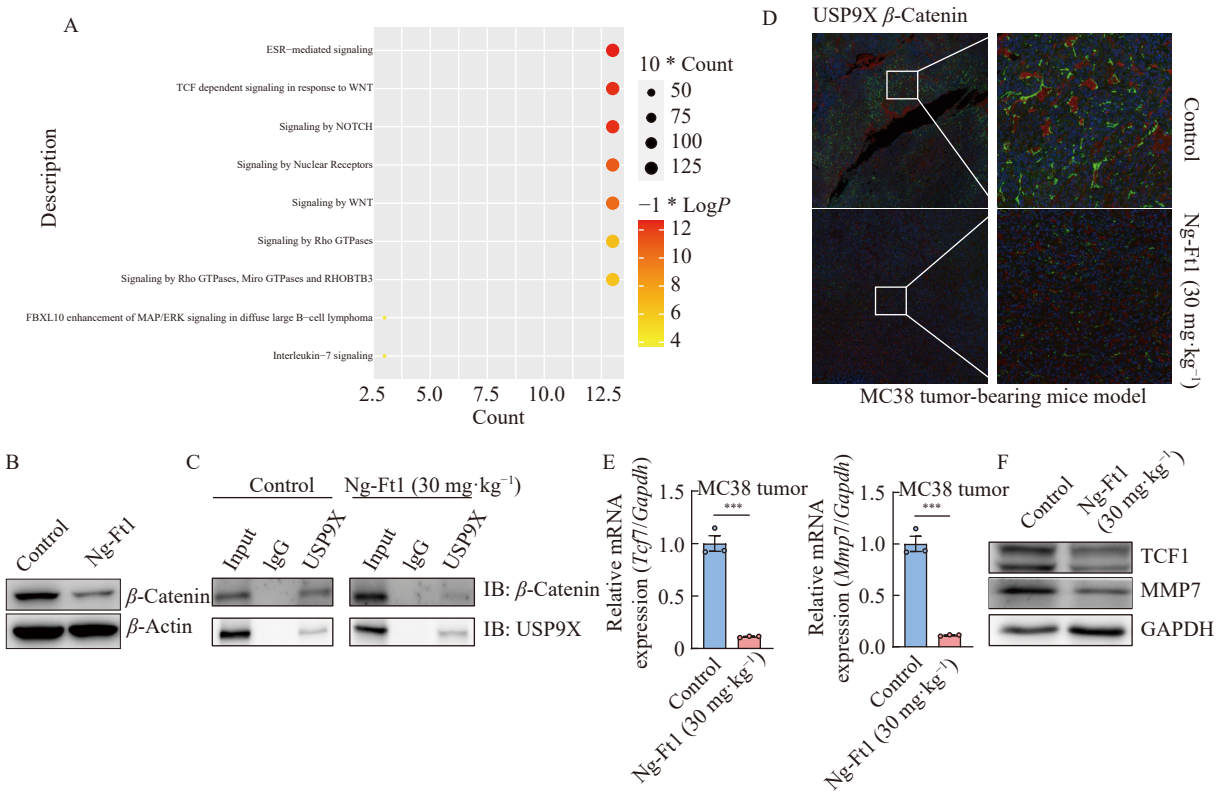

Fig. 6 Ng-Ft1 inhibits Wnt pathway activity by disrupting interactions between USP9X and *β*-catenin. (A) Signaling pathways correlated with USP9X upregulation in the TCGA CRC database. (B) The protein levels of USP9X and *β*-catenin are detected in CT26 cells. (C) Co-immunoprecipitation assay in total protein in CT26 cell line. (D) Co-localization of USP9X with *β*-catenin in MC38 tumor-bearing mouse tissues by immunofluorescence. (E) RT-qPCR shows mRNA level changes of Wnt pathway target genes *Tcf7* and *Mmp7*. (F) The protein levels of MMP7 and TCF1 are inhibited by Ng-Ft1 treatment. Data are presented as means ± SEM ($n = 3$). $^{***}P < 0.001$.

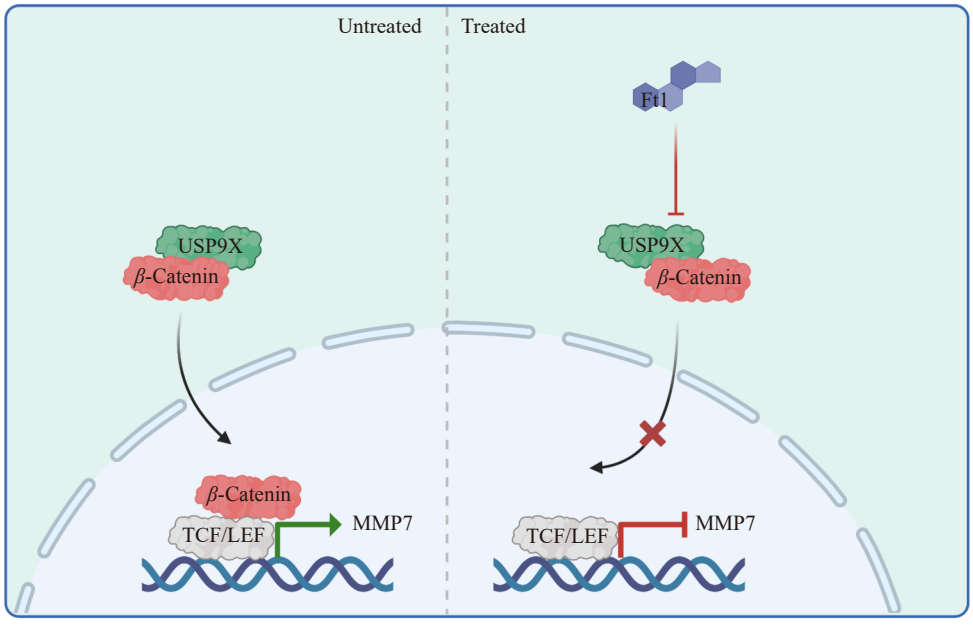

Fig. 7 Summary Chart. Ng-Ft1 specifically binds to USP9X in CRC cells, removes the protection of USP9X against *β*-catenin, and inhibits the transcriptional activity of downstream target genes of the Wnt signaling pathway. Created with BioRender.com.

target impacts. The development of more refined small-molecule inhibitors remains a research priority [37, 38]. Ng-Ft1, as a targeted Wnt inhibitor, markedly facilitates the degradation of *β*-catenin and reduces the expression of genes downstream

of the Wnt signaling pathway. Its efficacy indicates substantial promise for the targeted treatment of Wnt-associated tumors.

In our study, USP9X has been pinpointed as a direct target of Ng-Ft1, a protein known to be significantly involved in the progression of various cancers and in regulating tumor cell migration and cell function [39-42]. The exact impact of Ng-Ft1 on immune cells and its broader pharmacological mechanisms require further exploration. While USP9X is extensively expressed across normal and tumor tissues and Ng-Ft1's targeting of USP9X notably interferes with *β*-catenin, it is premature to conclude that this is the sole pharmacological mechanism behind Ng-Ft1's tumor-killing effects. Additional experiments, such as siRNA silencing, are necessary to confirm Ng-Ft1's dependency of Ng-Ft1 on USP9X. Although the anti-tumor mechanism of Ng-Ft1 has been demonstrated at both the transcriptional and translational levels, further research is essential to fully elucidate the significance of targeting USP9X with Ng-Ft1. Co-immunoprecipitation results indicating that Ng-Ft1 inhibits the Wnt signaling pathway by targeting USP9X and reducing its binding to *β*-catenin further support the mechanism by which Ng-Ft1 inhibits CRC cell growth.

The Wnt/*β*-catenin signaling pathway has recently been recognized for its significant role in modulating immune cell infiltration within the TME [43], thus affecting the response to immunotherapy. The inhibition of this pathway has been associated with an increased proportion of $CD8^+$ T cells and the initiation of invasion, potentially leading to more effective immune checkpoint suppression strategies [44]. USP9X, a crucial player in T cell development, significantly influences $CD8^+$ T cell functionality [45]. Moreover, PD-L1, a key molecule involved in immune evasion by tumors, is among the substrates deubiquitinated and thus stabilized by USP9X, facilitating tumor growth in conditions like oral squamous carcinoma [46]. Given these insights, it is plausible to suggest that Ng-Ft1 could improve the efficacy of immunotherapy. By enhancing $CD8^+$ T cell cytotoxicity, Ng-Ft1 may increase the response rates to immunotherapy treatments.

Supplementary Materials

Supplementary data to this article can be obtained by sending an E-mail to the corresponding authors.

References

[1] Siegel RL, Miller KD, Fuchs HE, *et al*. Cancer statistics [J]. *CA Cancer J Clin*, 2022, **72**(1): 7-33.

[2] Piawah S, Venook AP. Targeted therapy for colorectal cancer metastases: a review of current methods of molecularly targeted therapy and the use of tumor biomarkers in the treatment of metastatic colorectal cancer [J]. *Cancer*, 2019, **125**(23): 4139-4147.

[3] Benson AB, Venook AP, Al-Hawary MM, *et al*. NCCN Guidelines Insights: Colon Cancer, Version 2.2018 [J]. *J Natl Compr Canc Netw*, 2018, **16**(4): 359-369.

[4] Baxter NN, Kennedy EB, Bergsland E, *et al*. Adjuvant therapy for stage II colon cancer: ASCO guideline update [J]. *J Clin Oncol*, 2022, **40**(8): 892-910.

[5] Zhou J, Ji Q, Li Q. Resistance to anti-EGFR therapies in metastatic colorectal cancer: underlying mechanisms and reversal strategies [J]. *J Exp Clin Cancer Res*, 202, **40**(1): 328.

[6] Dong S, Liang S, Cheng Z, *et al*. ROS/PI3K/Akt and Wnt/*β*-catenin signalings activate HIF-1α-induced metabolic reprogramming to impart 5-fluorouracil resistance in colorectal cancer [J]. *J Exp Clin Cancer Res*, 2022, **41**(1): 15.

[7] Wang B, Tian T, Kall KH, *et al*. Targeting Wnt/*β*-catenin signaling for cancer immunotherapy [J]. *Trends Pharmacol Sci*, 2018, **39**(7): 648-658.

[8] Smith-Garvin JE, Koretzky GA, Jordan MS. T cell activation [J]. *Annu Rev Immunol*, 2009, **27**: 591-619.

[9] Wu Y, Hao X, Wei H, *et al*. Blockade of T-cell receptor with Ig and ITIM domains elicits potent antitumor immunity in naturally occurring HBV-related HCC in mice [J]. *Hepatology*, 2023, **77**(3): 965-981.

[10] Ducoin K, Oger R, Bilonda Mutala L, *et al*. Targeting NKG2A to boost anti-tumor CD8 T-cell responses in human colorectal cancer [J]. *Oncoimmunology*, 2022, **11**(1): 2046931.

[11] Wang B, Wang Y, Sun X, *et al*. CXCR6 is required for antitumor efficacy of intratumoral $CD8^+$ T cell [J]. *J Immunother Cancer*, 2021, **9**(8): e003100.

[12] Feng M, Zhao Z, Yang M, *et al*. T-cell-based immunotherapy in colorectal cancer [J]. *Cancer Lett*, 2021, **498**: 201-209.

[13] Tai D, Wells K, Arcaroli J, *et al*. Targeting the Wnt signaling pathway in cancer therapeutics [J]. *Oncologist*, 2015, **20**(10): 1189-1198.

[14] Steinhart Z, Pavlovic Z, Chandrashekhar M, *et al*. Genome-wide CRISPR screens reveal a Wnt-FZD5 signaling circuit as a druggable vulnerability of RNF43-mutant pancreatic tumors [J]. *Nat Med*, 2017, 23(1): 60-68.

[15] Kandoth C, McLellan M, Vandin F, *et al*. Mutational landscape and significance across 12 major cancer types [J]. *Nature*, 2013, **502**(7471): 333-339.

[16] Shi J, Li F, Luo M, *et al*. Distinct roles of Wnt/*β*-catenin signaling in the pathogenesis of chronic obstructive pulmonary disease and idiopathic pulmonary fibrosis [J]. *Mediators Inflamm*, 2017, **2017**: 3520581.

[17] Hu S, Wu Y, Zhao B, *et al*. *Panax notoginseng* saponins protect cerebral microvascularendothelial cells against oxygen-glucose deprivation/reperfusion-induced barrier dysfunction *via* activation of PI3K/Akt/Nrf2 antioxidant signaling pathway [J]. *Molecules*, 2018, **23**(11): 2781.

[18] Xiao Q, Kang Z, Liu C, *et al*. *Panax notoginseng* saponins attenuate cerebral ischemia-reperfusion injury *via* mitophagy-induced inhibition of NLRP3 inflammasome in rats [J]. *Front Biosci (Landmark Ed)*, 2022, **27**(11): 300.

[19] Li XM, Yuan DY, Liu YH, *et al*. *Panax notoginseng* saponins prevent colitis-associated colorectal cancer *via* inhibition IDO1 mediated immune regulation [J]. *Chin J Nat Med*, 2022, **20**(4): 258-269.

[20] Zhao Y, Sun X, Yu X, *et al*. Saponins from *Panax notoginseng* leaves improve the symptoms of aplastic anemia and aberrant immunity in mice [J]. *Biomed Pharmacother*, 2018, **102**: 959-965.

[21] Sun H, Ye Y, Pan Y. Immunological-adjuvant saponins from the roots of *Panax notoginseng* [J]. *Chem Biodivers*, 2005, **2**(4): 510-515.

[22] Qin HL, Wang XJ, Yang BX, *et al*. Notoginsenoside R1 attenuates breast cancer progression by targeting CCND2 and YBX3 [J]. *Chin Med J (Engl)*, 2021, **134**(5): 546-554.

[23] Lee CY, Hsieh SL, Hsieh S, *et al*. Inhibition of human colorectal cancer metastasis by notoginsenoside R1, an important compound from *Panax notoginseng* [J]. *Oncol Rep*, 2017,

37(1): 399-407.
[24] Chen JT, Li HZ, Wang D, *et al*. New dammarane monodesmosides from the acidic deglycosylation of notoginseng-leaf saponins [J]. *Helv Chim Acta*, 2006, **89**(7): 1442-1448.
[25] Gao B, Shi HL, Li X, *et al*. p38 MAPK and ERK1/2 pathways are involved in the pro-apoptotic effect of notoginsenoside Ft1 on human neuroblastoma SH-SY5Y cells [J]. *Life Sci*, 2014, **108**(2): 63-70.
[26] Qiu SP, Li HL, Shi HL, *et al*. Notoginsenoside Ft1 down-regulates HIF-1α, inhibits cell proliferation, decreases migration and promotes apoptosis in breast cancer cells [J]. *Acta Pharm Sin*, 2016, **51**(7): 1091-1097.
[27] Shen K, Ji L, Gong C, *et al*. Notoginsenoside Ft1 promotes angiogenesis *via* HIF-1α mediated VEGF secretion and the regulation of PI3K/AKT and Raf/MEK/ERK signaling pathways [J]. *Biochem Pharmacol*, 2012, **84**(6): 784-792.
[28] Xiong J, He J, Zhu J, *et al*. Lactylation-driven METTL3-mediated RNA m6A modification promotes immunosuppression of tumor-infiltrating myeloid cells [J]. *Mol Cell*, 2022, **82**(9): 1660-1677. e10.
[29] Xiao Y, Zhang T, Ma X, *et al*. Microenvironment-responsive prodrug-induced pyroptosis boosts cancer immunotherapy [J]. *Adv Sci (Weinh)*, 2021, **8**(24): e2101840.
[30] Kostic AD, Chun E, Robertson L, *et al*. Fusobacterium nucleatum potentiates intestinal tumorigenesis and modulates the tumor-immune microenvironment [J]. *Cell Host Microbe*, 2013, **14**(2): 207-215.
[31] Yang B, Zhang S, Wang Z, *et al*. Deubiquitinase USP9X deubiquitinates *β*-catenin and promotes high grade glioma cell growth [J]. *Oncotarget*, 2016, **7**(48): 79515-79525.
[32] Khan OM, Carvalho J, Spencer-Dene B, *et al*. The deubiquitinase USP9X regulates FBW7 stability and suppresses colorectal cancer [J]. *J Clin Invest*, 2018, **128**(4): 1326-1337.
[33] Yang L, Wang S, Pan Z, *et al*. TGFBR2 is a novel substrate and indirect transcription target of deubiquitylase USP9X in granulosa cells [J]. *J Cell Physiol*, 2022, **237**(7): 2969-2979.
[34] Dupont S, Mamidi A, Cordenonsi M, *et al*. FAM/USP9X, a deubiquitinating enzyme essential for TGFβ signaling, controls Smad4 monoubiquitination [J]. *Cell*, 2009, **136**(1): 123-135.
[35] Li T, Fu J, Zeng Z, *et al*. TIMER2.0 for analysis of tumor-infiltrating immune cells [J]. *Nucleic Acids Res*, 202, **48**(W1): W509-W514.
[36] Zhang Y, Wang X. Targeting the Wnt/*β*-catenin signaling pathway in cancer [J]. *J Hematol Oncol*, 2020, **13**(1): 165.
[37] Cui C, Zhou X, Zhang W, *et al*. Is *β*-catenin a druggable target for cancer therapy? [J]. *Trends Biochem Sci*, 2018, **43**(8): 623-634.
[38] Kahn M. Can we safely target the Wnt pathway? [J]. *Nat Rev Drug Discov*, 2014, **13**(7): 513-532.
[39] Garreau A, Blaize G, Argenty J, *et al*. Grb2-mediated recruitment of USP9X to LAT enhances themis stability following thymic selection [J]. *J Immunol*, 2017, **199**(8): 2758-2766.
[40] Naik E, Webster JD, DeVoss J, *et al*. Regulation of proximal T cell receptor signaling and tolerance induction by deubiquitinase Usp9X [J]. *J Exp Med*, 2014, **211**(10): 1947-1955.
[41] Naik E, Dixit VM. Usp9X is required for lymphocyte activation and homeostasis through its control of ZAP70 ubiquitination and PKCβ kinase activity [J]. *J Immunol*, 2016, **196**(8): 3438-3451.
[42] Park Y, Jin HS, Liu YC. Regulation of T cell function by the ubiquitin-specific protease USP9X *via* modulating the Carma1-Bcl10-Malt1 complex [J]. *Proc Natl Acad Sci USA*, 2013, **10**(23): 9433-9438.
[43] Pai SG, Carneiro BA, Mota JM, *et al*. Wnt/*β*-catenin pathway: modulating anticancer immune response [J]. *J Hematol Oncol*, 201, **10**(1): 101.
[44] Kalbasi A, Ribas A. Tumour-intrinsic resistance to immune checkpoint blockade [J]. *Nat Rev Immunol*, 2020, **20**(1): 25-39.
[45] Sheng L, Chen J, Tong Y, *et al*. USP9x promotes $CD8^+$ T-cell dysfunction in association with autophagy inhibition in septic liver injury [J]. *Acta Biochim Biophys Sin (Shanghai)*, 2022, **54**(12): 1-10.
[46] Wu JJ, Guo WZ, Wen DH, *et al*. Deubiquitination and stabilization of programmed cell death ligand 1 by ubiquitin-specific peptidase 9, X-linked in oral squamous cell carcinoma [J]. *Cancer Med*, 2018, **7**(8): 4004-4011.

Cite this article as: FENG Yutao, LI Yuan, MA Fen, WU Enjiang, CHENG Zewei, ZHOU Shiling, WANG Zhengtao, YANG Li, SUN Xun, ZHANG Jiwei. Notoginsenoside Ft1 inhibits colorectal cancer growth by increasing $CD8^+$ T cell proportion in tumor-bearing mice through the USP9X signaling pathway [J]. *Chin J Nat Med*, 2024, **22**(4): 329-340.